CrystEngComm

Accepted Manuscript

ROYAL SOCIETY OF CHEMISTRY

www.rsc.org/crystengcomm

CrystEngComm

PAPER

Ag embeded MnO nanorod: Facile synthesis and oxygen reduction

J. Liu, *[a] W. X. He,[a] X. J. Wei,[b] A.Q. Diao, [c] J.M. Xie[b] and X.M. Lü*[b]

Received 12th June 2015,
Accepted 00th January 20xx

DOI: 10.1039/x0xx00000x

www.rsc.org/crystengcomm

Using manganese(II) acetate tetrahydrate and silver salts as precursor, heterostructured Ag@$Ag_{1.8}Mn_8O_{16}$ nanocomposites were obtained by *in situ* redox reaction at room temperature. The molar ratio of Ag^+/Mn^{2+} was found to play an essential role in determining their morphology. At molar ratio of 1:200, the novel nanorod product with diameter of 10-20 nm and length of 280-800 nm was obtained. The nanorods were thermally unstable, further calcination leading to pure MnO nanorods embeded with Ag as the final product, which was demonstrated by analysis of XRD, TEM, Raman and XPS. TG and TEM analysis were also considered to explore the influence of calcination temperature and the molar ratio to the crystalline structure and the morphology of the synthesized product. The novel nanorod exhibited performance in oxygen reduction reaction (ORR), indicating a cost-effective electrocatalyst.

1. Introduction

The fabrication of one-dimensional (1-D) nanostructured materials, such as wires, belts, rods, and tubes, has attracted great amount of attention due to their unique properties and potential applications in catalysis, electronics and solar energy.[1] However, most research works are focused on synthesis of phase-pure 1-D nanostructured materials, including metal, metalloids,[2,3] metal oxides,[4] etc. Recently, the 1-D nanocomposites, such as binary and tertiary composite, have attracted considerable interest. The assembly of different nanomaterials with specific optical, magnetic, or electronic properties to multicomponent composites has shown advantage in chemical properties and enhanced catalytic performance in comparison with phase-pure 1-D materials.[5,6] Specifically tuning the structure and interface interactions within the nanocomposites has resulted in novel platforms of materials that may lead the way to various future technologies.[7-9]

Of the various kinds of nanomaterials, Manganese oxides (MnO_x) have attracted increasing attention. They are inexpensive, earth-abundant, environmentally benign, and have over 30 different crystal structures and variable valence of Mn centers in different polymorphs.[10-12] Many of them, such as MnO_2, Mn_2O_3, Mn_3O_4, amorphous MnO_x, have been widely studied as alternative ORR catalysts in alkaline solutions.[13] Unfortunately, pristine MnO_x usually exhibits limited ORR activities probably due to their low electrical conductivity.[14] Recently, a variety of appealing strategies have been used to solve these intractable problems, such as synthesizing MnO/C core-shell nanorods, coaxial MnO/C nanotubes, graphene-MnO composites.[15-17] Aharon Gedanken first prepared octahedral MnO and MnO/C core-shell nanoparticles and compared the electrochemical oxygen reduction reaction in alkaline electrolyte of the products with bulk MnO.[16] The MnO-composite electrode shows several-fold higher activity than the commercial bulk MnO electrode catalyst, indicating the better performance of the composite electrode over bulk MnO.

However, to prepare MnO, organic compounds would always be used. For example, oleic acid was used as precursor and high calcination temperature or harsh condition was adopted. These methods were complicated and could not reduce manganese precursor completely, leading to lower production. Herein, we for the first time report a facile method to prepare Ag embeded MnO nanorods through *in situ* redox reaction. The molar ratio of precursor, dropwise sequence and the calcination temperature were investigated to explore their influence to the structure, morphology and chemical properties. Also electrocatalytic performance of the Ag-MnO nanorods towards the ORR was investigated in detail.

2. Experimental

2.1. Materials

Manganese(II) acetate tetrahydrate ($Mn(CH_3COO)_2{\cdot}4H_2O$, 99%), silver nitrate ($AgNO_3$, 99%), silver acetate ($CH_3COOAg$, 99%) and polyvinylpyrrolidone (PVP, K-30) were purchased from Sinopharm Chemical Reagent CO., Ltd, China.

2.2. Synthesis of heterostructured Ag-MnO composites

[a] School of the Environment and Safety Engineering, Jiangsu University, Zhenjiang, 212013, Jiangsu, China
[b] School of Chemistry and Chemical Engineering, Jiangsu University, Zhenjiang, 212013,China
[c] Taizhou Polytechnic College, Taizhou, Jiangsu, 225300
Corresponding author: liujun1227@mail.ujs.edu.cn (J.Liu); laiyangmeng@163.com(X.M.Lü)
†Electronic Supplementary Information (ESI) available. See DOI: 10.1039/x0xx00000x

The 1-D heterostructured Ag-MnO nanorods were prepared as follows. Typically, PVP (55.6 mg) was added into $AgNO_3$ aqueous solution (10 mL, 10 mM) under stirring. After it was completely dissolved, the mixture was added into $Mn(CH_3COO)_2{\cdot}4H_2O$ (200 mM, 100 mL) aqueous solution by dripping. In the process, the solution gradually turned light grey. The mixture was then placed still overnight, and the precipitation was collected by centrifugation. Finally, the product was dried at 80 °C for 12 h. The resulting brown powder was further placed in quartz reactor and annealed in a vacuum tube type furnace (OTF-1200X, Wuhan, China) under nitrogen flowing. The temperature was programmed to rise at the rate of 20 °C/min from room temperature to the desired temperature. Other samples were also prepared at Ag^+/Mn^{2+} molar ratio of 1:0.25, 1:0.5, 1:1, 1:5, and 1:20 using desired Mn^{2+} concentration by the same procedure mentioned above.

2.3. Electrochemical measurements

The electrochemical measurements were performed in a three-electrode cell containing a glassy carbon rotating disk electrode (RDE), a platinum wire counter electrode, and a Hg/HgO reference electrode. The RDE (0.196 cm^2, Model MT134, Pine Instrument Co.) was polished with 0.5 μm alumina slurry and then washed with water and ethanol for several times. The electrolyte used in the tests was 0.1 M KOH. 5 mg catalysts were dispersed in 5 mL ethanol and ultrasonicated to form a brown solution. A sample of 20 μL of the mixture was pipetted onto prepared RDE, and then 5μL of 0.1 wt% nafion (in anhydrous ethanol) was further coated to protect the sample from detaching in the measurement process. Cyclic Voltammetry (CV) was carried out in electrolyte purged with saturated O_2 and N_2. The ORR activity of the catalysts was estimated using rotating disk in O_2 saturated electrolyte at a sweep rate of 5 $mV{\cdot}s^{-1}$. The O_2 flow was maintained bubbling in the electrolyte solution for continued O_2 saturation during the electrochemical measurements. All potentials were reported with respect to the reversible hydrogen electrode (RHE) scale in 0.1 M KOH.

2.4. Characterization

The as-prepared samples were characterized by X-ray diffraction (XRD) on a D/MAX-γAX diffractometer with Cu Kα radiation (λ = 1.5418 Å) operating at 40 kV and 200 mA with a scan rate of 8 °/min. The structure of heterostructured precursor and final product was further determined by Raman spectroscopy spectra (RSS) and the surface analysis was conducted by X-ray photoelectron spectroscopy (XPS). The morphologies of these samples were investigated with transmission electron microscopy (TEM) recorded on a TECNAI12 microscope operating at an acceleration voltage of 120 kV.

3. Results and discussion

3.1. Structure and morphology analysis

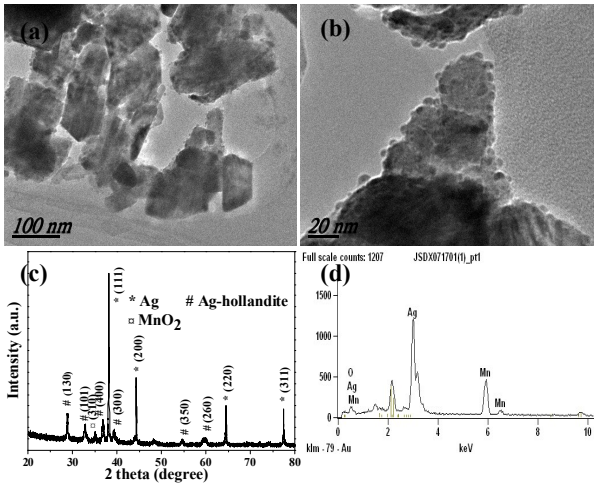

Fig. 1. TEM images (a, b), XRD (c), and energy dispersive X-ray EDX (d) of as-prepared nanocomposites at Ag/Mn molar ratio of 1:0.5.

Theoretically, the standard reduction potential of Ag^+/Ag (0.7996V) and MnO_2/Mn^{2+} (1.224V) is favourable for the generation of Ag and MnO_2 (equation 1), as the Gibbs free energy is negative and thus reaction is spontaneous.

$$2Ag^+ + Mn^{2+} + 2H_2O \rightarrow 2Ag + MnO_2 + 4H^+ \qquad (1)$$

Practically, we can't obtain the anticipated product according to the reaction equation. Figure 1(c) shows the XRD pattern of the nanocomposites prepared at Ag^+/Mn^{2+} molar ratio of 1:0.5 (equal to the reaction equation). The diffraction peaks are mainly assigned to the typical crystal structure of $Ag_{1.8}Mn_8O_{16}$ (hollandite, JCPDS, No.77-1987) and Ag (JCPDS, No.65-2871). A small XRD peak, located at 35.2°, conforms to the (310) plane of MnO_2 phase (JCPDS, No.72-1983). The $Ag_{1.8}Mn_8O_{16}$ phase with a measured lattice constant of a = 9.739 Å is the predominant component of the products. TEM image in Fig. 1a illustrates the lamellar substrate decorated with equally distributed Ag nanoparticles, and the magnified TEM image indicates Ag nanoparticles with sizes of ca. 4.66 nm, which is in accordance with the XRD calculation results(Fig. 1c, 2θ=38°, FWHM=0.038). The EDX spectroscopy, as shown in Fig. 1d, renders a rough estimation of Ag/Mn atom ratio of 1.11.

However, at the Ag^+/Mn^{2+} molar ratio of 1:200, uniform and regular 1-D architecture with diameters of 10-20 nm and lengths of 280-800 nm is obtained (Seen in Fig. 2). Furthermore, Ag particles with sizes of 0.8-2 nm are spotted equally on the surface of 1-D $Ag_{1.8}Mn_8O_{16}$ substrate, and fringe lattices of 2.36Å, HRTEM inset in Fig 2b, attribute to d(111) of Ag. Figure 2c indicates the growth of $Ag_{1.8}Mn_8O_{16}$ orientates along the [001] direction. It is reported that hollandite is unstable and readily decomposes to MnO_x.[18] Shen et al. have reported the fabrication of the single-atom Ag chains from silver nanoparticles supported on Hollandite-type manganese oxide nanorods. The dispersed Ag atoms of the silver

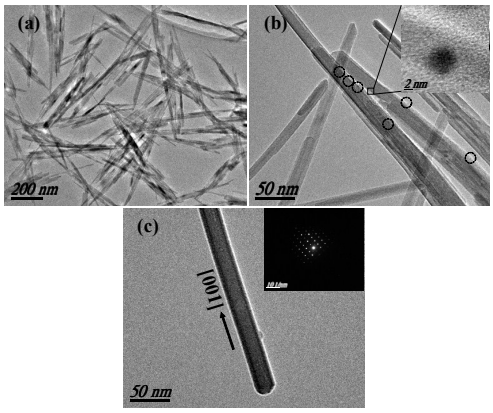

Fig. 2. TEM images of as-prepared nanocomposites at Ag/Mn molar ratio of 1: 200(a), amplified TEM image and HR-TEM image(inset) (b), amplified TEM image and SAED pattern(inset) (c).

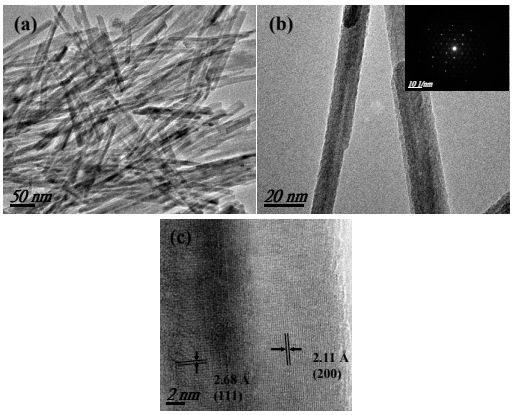

Fig. 4. TEM (a, b) and HR-TEM (c) images of 1-D Ag-MnO nanorods. Inset in (b): SAED pattern of one individual nanorod.

nanoparticles could thermally migrate along the external surfaces to the ends of the manganese oxide nanorods, and then consecutively inserted in the tunnels of the manganese oxide to form single-atom Ag chains, resulting in single Ag atoms anchored at the tunnel openings of the manganese oxide.[19] In our experiment, we also calcinate the sample synthesized at molar ratio of 1: 200 after *in situ* reaction to test its stability and structure based on the TG and XRD results (Fig. S1 in the ESI.†). Before calcination, the sample remains similar structure to other samples prepared at different molar ratio. After calcination, pure MnO phase (JCPDS, No.77-2363) is observed as the main phase, indicating that the composite nanorods transferred into MnO nanorods under high temperature calcination. The results were coherent with Raman spectroscopy analysis (Fig. S2 in the ESI.†). For further exploration, we calcinate the sample at 800 °C under N_2 flow. XRD patterns of the sample before and after calcination are shown in Fig. 3.

Figure 4 further shows the TEM images of the calcinated sample synthesized at molar ratio of 1: 200. Sharp peak of Ag (111) was found clearly in the calcinated nanorods in Fig. 3b. However, TEM images of the calcinated sample show that the supported Ag nanoparticle vagued after calcination (Fig. 4). The standard d(111) and d(200) fringe spacing of MnO is 2.56 and 2.22 Å, respectively, however, the d(111) and d(200) fringe lattices of our prepared MnO are 2.68, 2.11 Å. This deviation may be ascribed to the introduction of Ag atoms into MnO by ion exchange or substitution during calcination. According to the previous study of Shen group, we confer that these marginal amount of ultrafine Ag particles may transfer into MnO tunnel during the calcination process. Whatever, the introduction of silver would modify the physical and chemical properties of MnO nanorods.

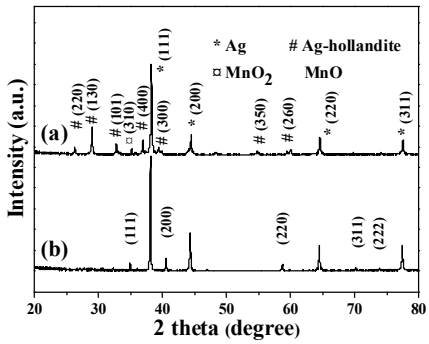

Fig. 3. XRD patterns of as-prepared nanocomposites at Ag/Mn molar ratio of 1:200 before (a) and after calcination (b).

Similar structure and morphology with 1-D structure can also be obtained using CH_3COOAg as precursor instead of $AgNO_3$ (Fig. S4 in the ESI.†). Interestingly, if we reverse the preparation procedure by dripping Mn^{2+} ions into Ag^+ ions, while keeping the other conditions unchanged, no product with distinct morphologies can be obtained. To further understand the detailed formation mechanism of the nanotubes, the molar ratio of Ag^+ to Mn^{2+} is changed while keeping the Ag^+ concentration constant. TEM and XRD results indicate that by adjusting the molar ratio of Ag/Mn precursor, similar structure but different morphology of the as-prepared nanocomposites is obtained. Scheme 1 illustrates their morphology under different condition. The main $Ag_{1.8}Mn_8O_{16}$ substrates with short lamellar shape are observed at the molar ratio of 1:0.25. As the concentration of Mn^{2+} increases to 5 mM at the molar ratio of 1:0.5, the average width of the nanolamellars changed from 60nm to 50nm. At 1:5 ratio, the average width of the nanolamellars further decreases to ca. 35nm. Also, the elongation of the substrate is noticeable. Further increasing Mn^{2+} concentration at 1:20 ratio, some one-dimension nanorod as the main product is obtained.

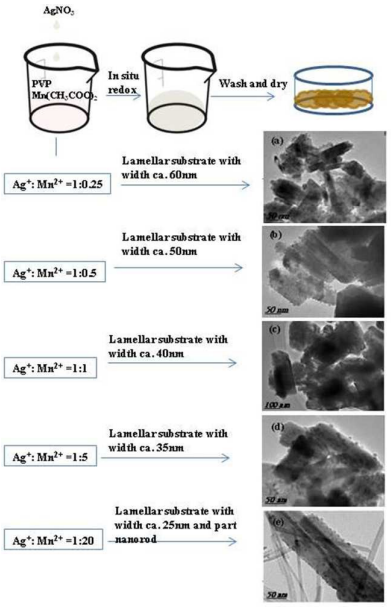

Scheme.1. Morphology change at different molar ratio.

Simultaneously, silver nanoparticles with average sizes varied from 5.98 to 3.88 nm are found highly dispersed on the surface of substrate with the decrease of the Ag^+/Mn^{2+} molar ratio. Therefore, it is possible to assume the growing mechanism of $Ag_{1.8}Mn_8O_{16}$ nanorobs as follows. By dripping $AgNO_3$ aqueous solution into $Mn(CH_3COO)_2{\cdot}4H_2O$ aqueous solution at room temperature, lamellar MnO_x species were initially formed. Because of the continuous addition of Ag^+, the lamellar structure of MnO_x could transfer into a lamellar structure of $Ag_{1.8}Mn_8O_{16}$. With the decrease of molar ratio, the tubular and curling lamellar structures gradually grew into nanorobs under improved ionic strength, and the lamellar particles decreased and finally disappeared. This phenomenon is similar to the formation of Ag-hollandite nanofibers from lamellar precursor.[19] These results also provide facile morphology-controlling strategy.

3.2. Surface analysis

Figure 5 displays the XPS spectra of Ag, Mn and O element oxidation states in the sample prepared at 1:200 before and after calcination. The XPS binding energies of Mn 2p in the samples before and after calcination are much similar. The binding energies of Mn $2p_{3/2}$ and Mn $2p_{1/2}$ are 640.70 and 653.39 eV, shifting to 640.57, and 652.50 eV after the sample annealed at 800 °C, respectively. While fitted with Shirly background and 20: 80 of Lorentzian: Gaussian convolution product shapes, the Mn $2p_{3/2}$ and Mn $2p_{1/2}$ can be further divided into three different peaks. The peaks at ~ 642.5, 641, and 640 eV of Mn $2p_{3/2}$ can be assigned to Mn^{4+}, Mn^{3+}, Mn^{2+}.[20-23] Since Mn^{4+}, Mn^{3+}, and Mn^{2+} share similar binding energies in the perovskite sample,[24] it is difficult to identify the manganese oxidation state just by the binding energy of Mn 2p. Hence, the XPS result of Mn 2p indicates that these as-

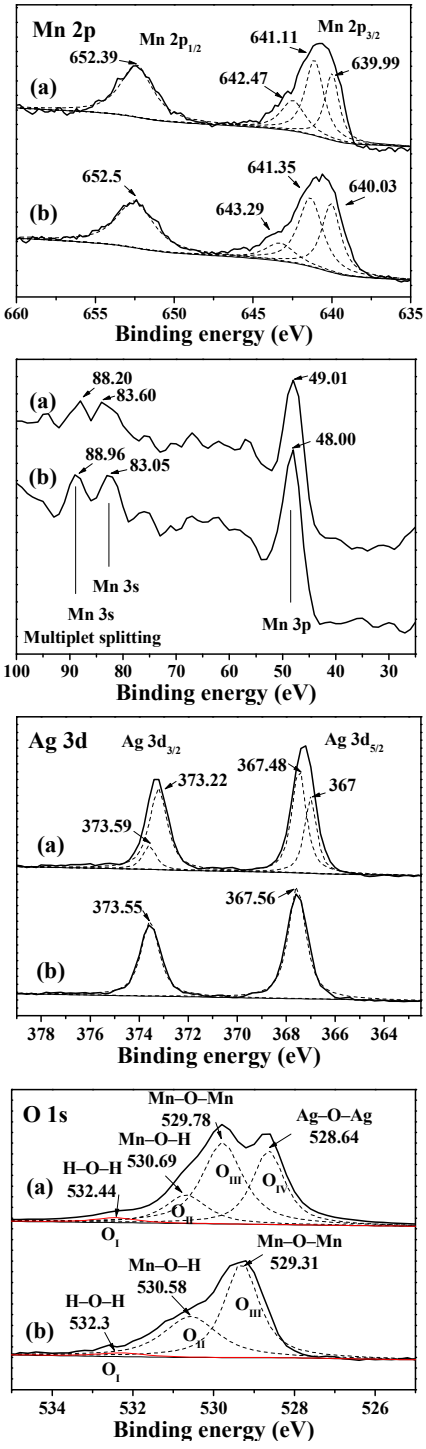

Fig. 5. XPS curves of Mn, Ag, and O elements in the as-prepared nanocomposites at Ag/Mn molar ratio of 1:200 before (a) and after annealed at 800 °C(b).

prepared samples may be composed of Mn^{4+}, Mn^{3+}, and Mn^{2+}. It is reported that Mn 3s favours the identification of manganese oxidation state, and the binding energy of the Mn 3s splitting decreases as the average manganese oxidation state increases.[25] The binding energy difference between the main peak and its satellite, denoted as ΔE3s, is 5.91 and 4.80 eV in sample before and after calcination. We then inferred that the manganese valances are estimated to be 3.57 and 2.09 in sample before and after calcination, respectively. The results indicate the presence of Mn^{3+} and Mn^{4+} in the sample after *in situ* synthetic process and manganese valances converted to +2 valence after the sample annealed at 800 °C. From the O 1s curve, it reveals that two multiple peaks changed to one single peak after annealing. The O 1s spectra could be divided into four individual peaks referring to H-O-H, Mn-O-H, Mn-O-Mn, Ag-O-Ag bands, denoted as O1, O2, O3, and O4 components, respectively. Component O1 with binding energy (BE) of 531~533 eV mostly belongs to be defect-oxide or hydroxyl-like groups.[26] Lower BE ca. 530 eV is assigned to O^{2-} species, including hydrated manganese (O2) and anhydrous compounds (O3). The peak at 528.64 eV is assigned to Ag-O-Ag (O4)[27], and the O4 peak shifts to higher binding energy at 529.31 eV after annealed.

Since no Ag^{+} peaks are observed after calcination at 800 °C, the peak at O3(529.31 eV) should be referred to Mn-O-Mn band. The Ag $3d_{3/2}$ and Ag $3d_{5/2}$ can be divided into two different peaks at 373.59, 373.22, 367.48, 367 eV, respectively. The peaks at 373 and 367eV can be ascribed to Ag $3d_{3/2}$ and Ag $3d_{5/2}$ of the metallic silver.[28] Based on the above analysis, it can be concluded that 1-D nanorods of $Ag/Ag_{1.8}Mn_8O_{16}$ converted into nanorods of Ag-MnO after annealed at 800 °C under N_2 atmosphere.

3.3. Ag-MnO nanorods as electrocatalyst for oxygen reduction reaction

There are two main pathways for the ORR in alkaline media: direct four-electron transfer and two-electron (stepwise) pathway. In four-electron transfer, oxygen is directly reduced: $O_2 + 2H_2O + 4e^- \rightarrow 4OH^-$ (1), whereas in the case of two-electron pathway, HO_2^- is produced as an intermediate: $O_2 + 2H_2O + 2e^- \rightarrow HO_2^- + OH^-$ (2a), $HO_2^- + H_2O + 2e^- \rightarrow 3OH^-$ (2b). Furthermore, the HO_2^- intermediate can undergo disproportionation according to: $HO_2^- \rightarrow OH^- + O_2$ (3). The kinetic of reaction 2b can be limiting, only with proper catalyst design, the hydroperoxide species can be recycled back into oxygen via disproportionation, thereby allowing for efficient use of the oxygen to achieve the pseudo four-electron reduction process (combination of eqs 2a and 3). To investigate the activity of ORR of the as-prepared samples, three typical Ag-MnO nano-heteroparticles prepared at Ag^{+}/Mn^{2+} molar ratio of 1:0.5, 1:5, and 1:200 were performed in 0.1M KOH aqueous solution at room temperature by using the catalysts modified RDEs. Figure 6a shows the cyclic voltammogram curves of these Ag-MnO nano-heteroparticles in the electrolyte saturated with N_2 and O_2. In the case of O_2 -

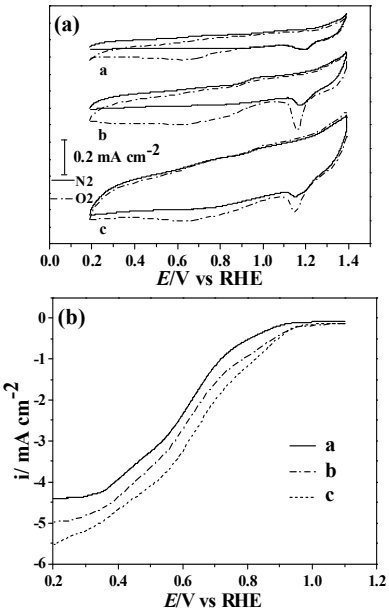

Fig. 6. a) Cyclic voltammograms of Ag-MnO nano-heteroparticles prepared with Ag^{+}/Mn^{2+} molar ratio of 1:0.5 (a), 1:5 (b), and 1:200 (c) in N_2-saturated (solid curves) and O_2- saturated (dashed curves) 0.1 M KOH. b) The corresponding RDE polarization curves recorded in 0.1 M KOH saturated with O_2 at a sweep rate of 5 mVs^{-1} and a rotation rate of 1600 rpm.

saturated KOH solution, these Ag-MnO nano-heteroparticles show a cathodic peak near 0.95 V (vs. HRE), which is more positive than the reported pure MnO catalysts with a cathodic peak at 0.56 V, indicating Ag-MnO nano-heteroparticles are more active than pure MnO catalysts.[29] Furthermore, the cathodic peak potential of Ag-MnO nanorods(prepared at molar ratio of 1:200) composite catalyst is more positive than that of MnO_x-Ag electrocatalysts(typically negative than 0.75V),[30] highlighting low overpotential for ORR and excellent oxygen reduction ability of Ag-MnO composite catalyst.

A set of polarization curves for ORR of Ag-MnO nanorods(prepared at molar ratio of 1:200) collected from 100 to 1600 rpm are shown in Fig. 7. The diffusion limited current density increases with the rotation speed increases, and the Koutecky-Levich plots (i^{-1} vs $\omega^{-1/2}$) are deduced from polarization curve at different potentials. The value of electron transfer number, n, is determined by using the Levich equation as follows: $i=0.620nFAC D^{2/3}\omega^{1/2}v^{-1/6}$, where i is the diffusion limited current, A is the area of the electrode, C is the concentration of oxygen saturated 0.1 M KOH at room temperature, ω and v is the rotation rate and the kinetics viscosity, respectively. The electron transfer number of Ag-MnO nanorods is calculated to be 3.43, approaching the four-electron transfer. As former studies reported MnO_x can readily catalyze reaction 2a but is slow for HO_2^- disproportionation.[31] To fulfill the four-electron pathway, the hydroperoxide species must be recycled back into oxygen via disproportionation.

However, MnO_x alone does not fully catalyze the complete four-electron reduction of oxygen. To further enhance the catalytic activity, MnO_x may be mixed with an active transition metal.[32] Silver is a moderately efficient electronic conductor and can catalyzes the direct four-electron ORR, though there is a large overpotential associated with the first two-electron transfer (eq. 2a).[33] Composties of MnO and Ag have the potential to enhance catalytic activity, whereby Ag catalyzes direct oxygen reduction(eq. 2a) and MnO catalyze direct disproportionation the hydroperoxide intermediate(eq. 3).[34,35] Hence, the novel nanorods of MnO embeded with Ag exhibit synergistic effect, which influence catalysis of various reaction steps and ensemble effects from Ag-MnO sites for the multistep reaction network.

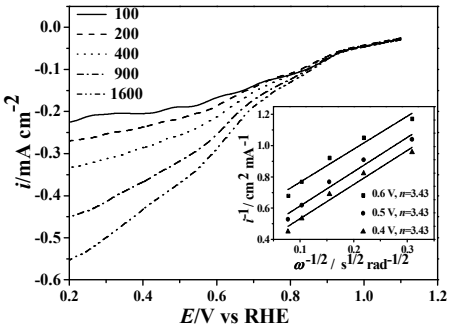

Fig. 7. ORR polarization curves for Ag-MnO nanorods at the different rotation rates, and the inset is Koutecky-Levich plots at different potentials.

4. Conclusions

In summary, we present a simple *in situ* template-free strategy to synthesize nanorod composite precursor loaded with Ag nanoparticles. Dripping Ag^+ into Mn^{2+} of different concentration leads to different morphology of composite product. At Ag^+/Mn^{2+} molar ratio of 1:200, nanorod precursor with diameters of 10-20 nm and lengths of 280-800 nm were obtained. After calcination at 800 °C, Ag embeded pure MnO hybrid composites with similar morphology of its precursor was formed. The Ag-MnO nanocomposites show effective electro-catalysis in ORR, which reaches 3.43 electrons transfer number, indicating a cost-effective catalyst. Besides, such *in situ* template-free strategy shows a promising vista to synthesize metal/metal oxide 1-D structure.

Acknowledgements

We acknowledge the financial supports of the National Natural Science Foundation (NO. 21003065), and Jiangsu Province Research Joint Innovation Fund-Prospective Joint Research Project (BY2014123-08).

References

1 Y. N. Xia, P. D. Yang, Y. G. Sun, Y. Y. Wu, B. Mayers, B.Gates, Y. D. Yin, F. Kim and H. Q. Yan, *Adv. Mater*., 2003, **15**, 353.
2 L. Vigderman, B. P. Khanal and E. R. Zubarev, *Adv. Mater.,* 2012, **24**, 4811.
3 Y. N. Xia YN, Y. J. Xiong, B. Lim, S. E. Skrabalak, *Angew. Chem. Int. Ed*., 2009, **48**, 60.
4 Q. Wang, Z. H. Wen and J. H. Li, *Inorg. Chem*., 2006, 2006, **45**, 6944.
5 J. Du, J. Zhang, Z. Liu, B. Han, T. Jiang and Y. Huang, *Langmiur,* 2006, **22**, 1307.
6 H. G. Yang and H. C. Zeng, *J. Am. Chem. Soc*. ,2005, **127**, 270.
7 S. Yang, Z. Peng and H. Yang, *Adv. Funct. Mater.,* 2008, **18**, 2745.
8 Q. Liu, Z. Yan, N. L. Henderson, J. C. Bauer, D. W. Goodman, J. D. Batteas and R. E. Schaak, *J. Am. Chem. Soc.,*2009, **131**, 5720.
9 B. Lim, M. Jiang, P. H. C. Camargo, E. C. Cho, J. Tao, X. Lu, Y. Zhu and Y. Xia, *Science*, 2009, **324**,1302.
10 H. Y. Zhang, Y. Xie, Z. Y. Sun, R. T. Tao, C. L. Huang, Y. F. Zhao and Z. M. Liu, *Langmuir*, 2011, **27**, 1152.
11 C. J. Morten and T. F. Jamison, *J. Am. Chem. Soc.,* 2009, **131**, 6678.
12 X. Yu, J. He, D. Wang, Y. Hu, H. Tian and Z. He, *J. Phys. Chem. C*, 2012, **116**, 851.
13 Y. Gorlin, C. J. Chung, D. Nordlund, B. M. Clemens and T. F. Jaramilo, *ACS Catal*. 2012, **2**, 2687.
14 Y. M. Tan, C. F. Xu, G. X. Chen, X. L. Fang, N. F. Zheng and Q. G. Xie, *Adv. Funct. Mater.,* 2012, **22**, 4584.
15 Y. J. Mai, D. Zhang, Y. Q. Qiao, C. D. Gu, X. L. Wang and J. P. Tu, *J. Power Sources,*2012*,* **216**, 201.
16 S. Shanmugam and A. Gedanken, *J. Phys. Chem. B*, 2006, **110**, 24486.
17 S. M. Lee, S. H. Choi and J. K. Lee, *Electrochim. Acta*, 2014,**132**, 441.
18 L. Demarconnay, C. Coutanceau and J. M. Léger, *Electrochim. Acta*, 2004, **49**, 4513.
19 J. L. Chen, X. F. Tang, J. L. Liu, E. S. Zhan, J. Li, X. M. Huang and W. J. Shen, *Chem. Mater.,*2007*,* **19**, 4292.
20 Z. W. Huang, X. Gu, Q. Q. Cao, P. P. Hu, J. M. Hao, J. H. Li JH and X. F. Tang, *Angew. Chem. Int. Ed*., 2012,**124**, 4274.
21 S. H. Liang, F. Teng, G. Bulgan, R. L. Zong, Y. F. Zhu, *J. Phys. Chem. C,*2008, **112**, 5307.
22 Q. Feng, H. Kanoh, Y. Miyai, K. Ooi, *Chem. Mater.,*1995*,* **7**, 148.
23 M. A. Langell, C. W. Hutchings, G. A. Carson and M. H. Nassir, *J. Vac. Sci. Technol. A,* 1996, **14**, 1656.
24 A. A. Audi and M. A. Sherwood, *Surf. Interface. Anal*., 2002, **33**, 274.
25 M. Chigane and M. Ishikawa, *J. Electrochem. Soc*., 2000, **147**, 2246.
26 V. R. Galakhov VR, M. Demeter, S. Bartkowski, M. Neumann M, N. A. Ovechkina, E. Z. Kurmaev, N. I. Lobachevskaya, Y. M. Mukovskii, J. Mitchell and D. L. Ederer, *Phys. Rev. B*, 2002, **65**, 113102.
27 S. Hamoudi, F. Larachi, A. Adnot and A. Sayari, *J. Catal.,* 1999, **185**, 333.
28 T. Suzuki-Muresan, J. Vandenborre, A. Abdelouas, B. Grambow and S. Utsunomiya, *J. Nucl. Mater.,* 2011, **419**, 281.

29 L. H. Tjeng, M. B. J. Meinders, J. Elp, J. Ghijsen and G. A. Sawatzky, *Phys. Rev. B*, 1990, **41**, 3190.

30 Y. Tan, C. Xu, G. Chen, X. Fang, N. Zheng and Q. Xie, *Adv. Funct. Mater.*, 2012, **22**, 4584.

31 M. A. Kostowskyj, D. W. Kirk, S. J. Thorpe, *Int. J. Hydrogen. Energ.,* 2010, **35**, 5666.

32 F. H. B. Lima, J. Zhang, M. H. Shao, K. Sasaki, M. B. Vukmirovic, E. A. Ticianelli EA and R. R. Adzic, *J. Phys. Chem. C*, 2007, **111**, 404.

33 F. H. B. Lima, M. L. Calegaro and E. A. Ticianelli, *J. Electroanal. Chem.,* 2006, **590**,152.

34 D. A. Slanac, A. Lie, J. A. Paulson, K. J. Stevenson and K. P. Johnston, *J. Phys. Chem. C*, 2012, **116**, 11032

35 N. Ominde, N. Bartlett, X. Yang and D. Qu, J. Power Source, 2010, **195**, 3984.

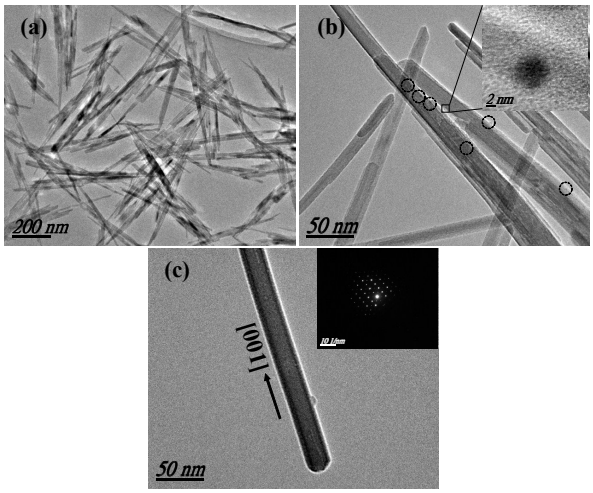

TEM images of as-prepared nanocomposites under Ag/Mn molar ratio of 1/200. Inset in (b): HR-TEM image taken from image (b), (c): SAED pattern taken from one individual nanorod